

Simulations of momentum feedback by black hole winds

Sergei Nayakshin^{1,2} and Chris Power¹

¹ *Department of Physics & Astronomy, University of Leicester, Leicester, LE1 7RH, UK*

² *Max-Planck-Institut für Astrophysik, Karl-Schwarzschild-Strasse 1, D-85741, Garching, Germany*

Accepted 2008 ?? ??. Received 2008 ?? ??; in original form 2008 05 ??

ABSTRACT

The observed super-massive black hole (SMBH) mass – galaxy velocity dispersion ($M_{\text{bh}} - \sigma$) correlation may be established when winds/outflows from the SMBH drive gas out of the potential wells of classical bulges. Here we present numerical simulations of this process in a static isothermal potential. Simple spherically symmetric models of SMBH feedback at the Eddington luminosity can successfully explain the $M_{\text{bh}} - \sigma$ and nuclear cluster mass $M_{\text{NC}} - \sigma$ correlations, as well as why larger bulges host SMBHs while smaller ones host nuclear star clusters. However these models do not specify how SMBHs feed on infalling gas whilst simultaneously producing feedback that drives gas out of the galaxy.

More complex models with rotation and/or anisotropic feedback allow SMBHs to feed via a disc or regions not exposed to SMBH winds, but in these more realistic cases it is not clear why a robust $M_{\text{bh}} - \sigma$ relation should be established. In fact, some of the model predictions contradict observations. For example, an isotropic SMBH wind impacting on a disc (rather than a shell) of aspect ratio $H/R \ll 1$ requires the SMBH mass to be larger by a factor $\sim R/H$, which is opposite to what is observed. We conclude that understanding how a SMBH feeds is as important a piece of the puzzle as understanding how its feedback affects its host galaxy.

Finally, we note that in aspherical cases the SMBH outflows induce differential motions in the bulge. This may pump turbulence that is known to hinder star formation in star forming regions. SMBH feedback thus may not only drive gas out of the bulge but also reduce the fraction of gas turned into stars.

Key words: Galaxy: centre – accretion: accretion discs – galaxies: active

1 INTRODUCTION

It is believed that the centres of most galaxies contain super-massive black holes (SMBHs) whose mass M_{bh} correlates with the velocity dispersion σ of the host galaxy (Ferrarese & Merritt 2000; Gebhardt et al. 2000; Tremaine et al. 2002). Similarly, there is a correlation between M_{bh} and the mass of the bulge, M_{bulge} for large SMBH masses (Magorrian et al. 1998; Häring & Rix 2004; Gültekin et al. 2009). Observations also suggest that the masses of nuclear star clusters (NC) ($10^5 M_{\odot} \lesssim M_{\text{NC}} \lesssim 10^8 M_{\odot}$) correlate with the properties of their host dwarf ellipticals (Ferrarese et al. 2006; Wehner & Harris 2006) in a manner that is analogous to the one between SMBHs and their host ellipticals.

These empirical relations can be explained in a very natural way if the growth of host galaxies and their central SMBHs or NCs are linked by feedback. This was first pointed out by Silk & Rees (1998), who highlighted the potential importance of SMBH heating and outflows before any robust observational evidence for such a link had been found. Sub-

sequently, Fabian (1999) argued that radiation pressure acting on cold gaseous clouds in the bulge could give rise to the observed correlations. King & Pounds (2003) argued for the existence sub-relativistic outflows from the very central regions of AGN, which prompted King (2003, 2005) to study the motion of a shell of gas swept up by a wind/outflow from a central black hole in a galactic isothermal dark matter potential. King (2005) demonstrated that the shell will be expelled from the potential provided the black hole mass exceeds a critical value that, as a function of σ , turns out to be close to the observed $M_{\text{BH}} - \sigma$ relation.

The main result of King (2003, 2005) can be deduced using a simpler order of magnitude “weight argument”. According to this argument, the SMBH luminosity is assumed to be limited by the Eddington value. Radiation pressure drives a wind. King & Pounds (2003) argue that wind velocity is comparable to the escape velocity from the inner accretion disc, e.g., $v \sim 0.1c$. The momentum outflow rate is assumed to be

$$\dot{P}_{\text{SMBH}} \approx \frac{L_{\text{Edd}}}{c} = \frac{4\pi G M_{\text{BH}}}{\kappa}; \quad (1)$$

here κ is the electron scattering opacity and M_{BH} is the SMBH mass. This result is natural to the order of magnitude: L_{Edd}/c is the radiation momentum flux which is presumably passed to the wind as radiation accelerates the outflow (cf. King & Pounds 2003). The argument also assumes that the black hole wind is optically thin at the point of interaction with the ambient gas. Because the cooling time of the shocked gas is short on scales appropriate for observed bulges (King 2003, 2005), the bulk energy of the outflow is thermalised and quickly radiated away. It is then only the momentum push (equation 1) of the outflow on the ambient gas that is important since it is this that produces the outward force on the gas (as in the earlier model by Fabian 1999). The weight of the gas is $W(R) = GM(R)[M_{\text{total}}(R)]/R^2$, where $M_{\text{gas}}(R)$ is the enclosed gas mass at radius R and $M_{\text{total}}(R)$ is the total enclosed mass including dark matter. For an isothermal potential, $M_{\text{gas}}(R)$ and $M_{\text{total}}(R)$ are proportional to R , so the result is

$$W = \frac{4f_g\sigma^4}{G}. \quad (2)$$

Here f_g is the baryonic fraction and $\sigma^2 = GM_{\text{total}}(R)/2R$ is the velocity dispersion in the bulge. By requiring that momentum output produced by the black hole just balances the weight of the gas, it follows that

$$M_\sigma = \frac{f_g\kappa}{\pi G^2}\sigma^4, \quad (3)$$

which is consistent with the observed the $M_{\text{BH}}-\sigma$ relation.

To order of magnitude, relation 2 should hold for any potential at the virial radius. Therefore the model by King (2003, 2005) appears to be a promising explanation of the observed correlations between SMBHs and their host galaxies. However, additional complications, not considered in King (2003, 2005), may be important. Amongst these are (1) the self-gravity of the gas, because gas that accumulates at the centre of the potential may begin to dominate it and therefore alter the result; (2) finite angular momentum of the gas may lead to formation of a disc; (3) collimated and variable outflows.

The goal of this paper is to verify that the predictions of the analytical model of King (2003, 2005) hold and to explore more realistic settings, of the kind just described. Note that we concentrate on the early stages of galaxy evolution, when we would expect galaxies to be gas-rich and the baryonic mass within dark matter haloes is dominated by gas rather than stars. At later times, when the SMBH is likely to be less luminous and the galaxy is less gas-rich, we would expect different forms of feedback to become important, such as relativistic jets and the associated radio bubbles (e.g., Churazov et al. 2002) or pre-heating due to the inverse Compton effect (e.g., Sazonov et al. 2005). However, we do not include these forms of feedback in our current simulations.

2 FIXED BH MASS RUNS

2.1 Numerical method

Nayakshin et al. (2009a) developed a new method for ra-

diation transfer in SPH based on Monte Carlo packets, which can also be used to simulate winds in the momentum-conserving phase. As discussed in the Introduction, one can consider only the momentum transfer from the outflow to the ambient gas in this regime. In addition, for the problem at hand, the typical velocity of the ambient gas is of the order the velocity dispersion in the bulge, which is less than a few 100 km/sec. In contrast, the black hole outflow is much faster, $v \sim 0.1c$, which implies that the mass of the black hole wind is negligibly small compared with that of the gas in the bulge at the point there the latter is driven away. Hence we can neglect the mass of the black hole wind in comparison to that of the ambient medium.

Accordingly, we use massless particles moving with velocity $v = 0.1c$ to simulate the black hole wind. The wind particles propagate in straight lines until they encounter one or more SPH particles at which point they transfer their momentum to the particles. For more information on the method and validation of the code see Nayakshin et al. (2009a), especially their §3.

For spherically symmetric tests, we use 35,000 SPH particles. The wind particles carry momentum $p_{\text{wind}} = 0.1m_{\text{sph}}\sigma$ each. This satisfies the requirement $p_{\text{wind}} \ll p_{\text{sph}}$, where p_{sph} is the typical SPH particle momentum ($\sim m_{\text{sph}}\sigma$ here), and ensures that Poisson noise from our Monte Carlo scheme is small enough not to compromise our results (see Nayakshin et al. 2009a). The particles are emitted by the black hole at the rate

$$\dot{N}_{\text{wind}} = \frac{L_{\text{Edd}}}{c p_{\text{wind}}}, \quad (4)$$

where L_{Edd} is the Eddington luminosity for the black hole. They are ejected isotropically unless stated otherwise.

We perform our simulations in a static singular isothermal sphere potential with velocity dispersion $\sigma = 147 \text{ km s}^{-1}$. The units of mass and distance are $M_U = 10^{10} M_\odot$ and $R_U = 1 \text{ kpc}$ respectively; the unit velocity is $V_U = \sqrt{GM_U/R_U} = \sqrt{2}\sigma$. Equation 3 yields the expected value for the critical mass at which gas should be expelled;

$$M_\sigma = \frac{f_g\kappa}{\pi G^2}\sigma^4 = 1.1 \times 10^8 M_\odot. \quad (5)$$

To check this prediction, we first limit our simulations to spherically symmetric initial conditions. We work with a finite extent shell since that allows us to explore interesting regions of parameter space. The initial radial distribution of gas follows the distribution of dark matter, assumed to dominate the potential: $\rho(R) \propto R^{-2}$ for $R_{\text{in}} < R < R_{\text{out}}$. For all the tests in this paper, $R_{\text{in}} = R_{\text{out}}/2$. As in King (2003, 2005), the normalisation of gas density, and hence the mass of the shell, is set by the cosmological baryon mass fraction, $f_{g0} = \rho_g/\rho_{\text{total}} \simeq 0.16$, where $\rho_{\text{total}} = \rho_{\text{DM}} + \rho_g$ is the total mass density, and ρ_g and ρ_{DM} are the gas and dark matter densities, respectively. For the isothermal potential, $\rho_{\text{total}}(R) = \sigma^2/2\pi GR^2$. Because our focus is momentum feedback, we adopt the isothermal equation of state for the gas, assuming $T = 3 \times 10^5 \text{ K}$. This is lower than the virial temperature, $T_{\text{vir}} \approx 10^6 \text{ K}$, for the potential we are using, preventing small scale gas fragmentation. The latter process would lead to star formation and feedback from star formation, in both heating and momentum-driven forms. We plan to include these processes in our future work, for now

neglecting them in comparison with the SMBH feedback altogether.

We set $R_{\text{acc}} = 0.5$ as the inner boundary of our computational domain. SPH particles that cross inside this inner boundary are removed. Note however that this scale is still too large to associate it with SMBH accretion directly, and there is no model-independent parameter-free way of connecting this “sunken” mass with SMBH accretion and feedback. For simplicity we take the pragmatic approach in this paper and consider only tests in which the black hole feedback is either constant or increases at a rate fixed by the Eddington limit. This allows us to concentrate on gas dynamics without worrying about the complexities of the non-linear and model-dependent accretion-feedback link. The “accreted” gaseous mass is thus considered to be mainly used in star formation inside R_{acc} and the feedback from that is neglected.

Before we begin the discussion of results, we show in Figure 1 two typical snapshots from the spherically symmetric calculations. These show gas column densities in an angle-slice projection. Specifically, the gas column density shown in the Figure 1, and in all similar figures below, is calculated by

$$\Sigma(x, y) = \int_{-z(x, y)}^{z(x, y)} \rho(x, y) dz, \quad (6)$$

where the limits of the integration are given by $z(x, y) = r \tan \xi$, and $r = (x^2 + y^2)^{1/2}$. The angle ξ is chosen to be $\tan \xi = 1/4$ for this paper. This projection method is convenient as it permits an unobstructed view into the central regions where the black hole resides. Had we used a constant thickness $z(x, y) = \text{const}$ projection method, then either the innermost region would not have been resolved sufficiently or an insufficient number of the SPH particles in the outermost regions would have been sampled for a statistically meaningful figure.

The tests shown in Figure 1 are described in §2.3 (left panel) and §2.4 (right panel). Briefly, the former has $M_{\text{bh}} = 2 \times 10^8 M_{\odot}$, whereas the latter has $M_{\text{bh}} = 4 \times 10^8 M_{\odot}$. In both cases the gas is falling in with radial velocity $v_r = -1$ (in code units) initially. In the lighter SMBH case, the black hole momentum outflow is insufficient to reverse the shell’s infall and it engulfs the black hole. In the right panel, on the other hand, the initially thick shell is first compressed to a thinner shell by the opposing actions of the black hole outflow and the inward inertia of the outer layers, and then expelled to infinity.

2.2 Initially static shell tests

We begin with tests in which gas is initially at rest (even though this is unrealistic for the chosen temperature). The initial outer radius of the shell is $R_{\text{out}} = 40$ kpc for these runs. Figure 2 shows results of three such tests, where we vary the black hole mass from $M_{\text{bh}} = 5 \times 10^7 M_{\odot}$ to $M_{\text{bh}} = 2 \times 10^8 M_{\odot}$ by factors of 2. We define a mean radius and velocity of the gas by averaging over all the SPH particles in a simulation. Defined in this way, the “shell” radius is plotted in units of the initial mean radius, whereas the velocity is shown in code units. It is apparent from Fig-

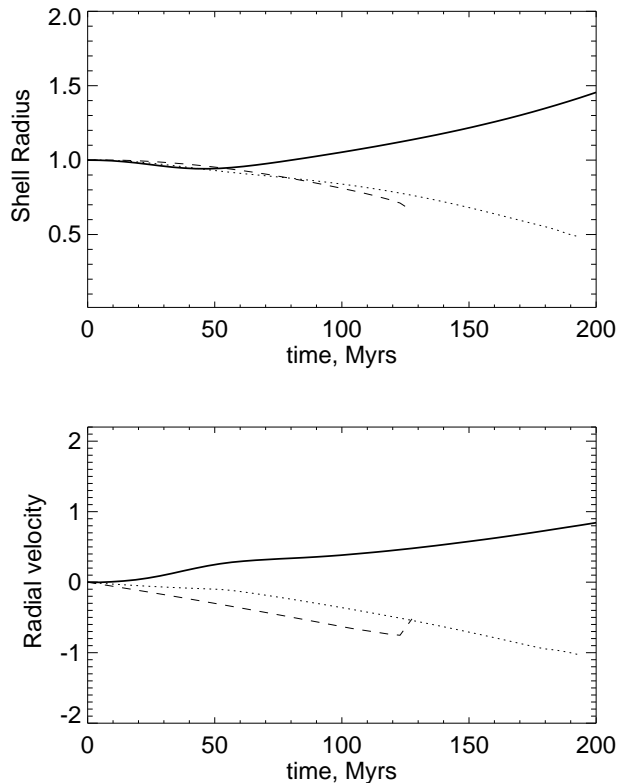


Figure 2. Mean radius (upper panel) and radial velocity (lower panel) of the gas as a function of time for three different black hole masses: $M_{\text{bh}} = 2 \times 10^8 M_{\odot}$, solid, $M_{\text{bh}} = 10^8 M_{\odot}$, dotted, and $M_{\text{bh}} = 5 \times 10^7 M_{\odot}$, dashed. The radius is plotted in units of the initial mean radius, whereas velocity is shown in code units ($\sqrt{2}\sigma$). See §2.2 for more detail.

ure 2 that the lower mass black holes ($M_{\text{bh}} \leq 10^8 M_{\odot}$) are unable to expel the shell of gas, whereas the more massive black hole ($M_{\text{bh}} \leq 2 \times 10^8 M_{\odot}$) is able to expel the shell. We therefore estimate that the critical black hole mass for this potential is around $1.5 \times 10^8 M_{\odot}$, in a very good agreement with the estimate in equation 5.

2.3 Initially infalling shell, $M_{\text{bh}} = 2 \times 10^8 M_{\odot}$

This simulation is identical to that presented in §2.2 with $M_{\text{bh}} = 2 \times 10^8 M_{\odot}$, except the radial velocity of gas is now non-zero, with $v_r = -1$. The additional initial inertia of the shell suggests that the critical M_{σ} mass should be higher in this case, which turns out to be true.

Figure 3 shows the mean shell radius, R_{sh} , in units of its initial value (dash-dotted green curve) as a function of time. The inward motion of the shell cannot be prevented in this simulation, as is clearly indicated by the monotonically decreasing mean radius. The solid curve shows the mean radial velocity of the gas scaled to its initial value. The shell is slightly decelerated initially by the momentum of the SMBH outflow, i.e., $|v_r|$ decreases until $t \sim 40$ Myrs. However, at $t \sim 40$ Myrs the shell starts to accelerate and falls “onto” the SMBH, completely enveloping it. To follow the evolu-

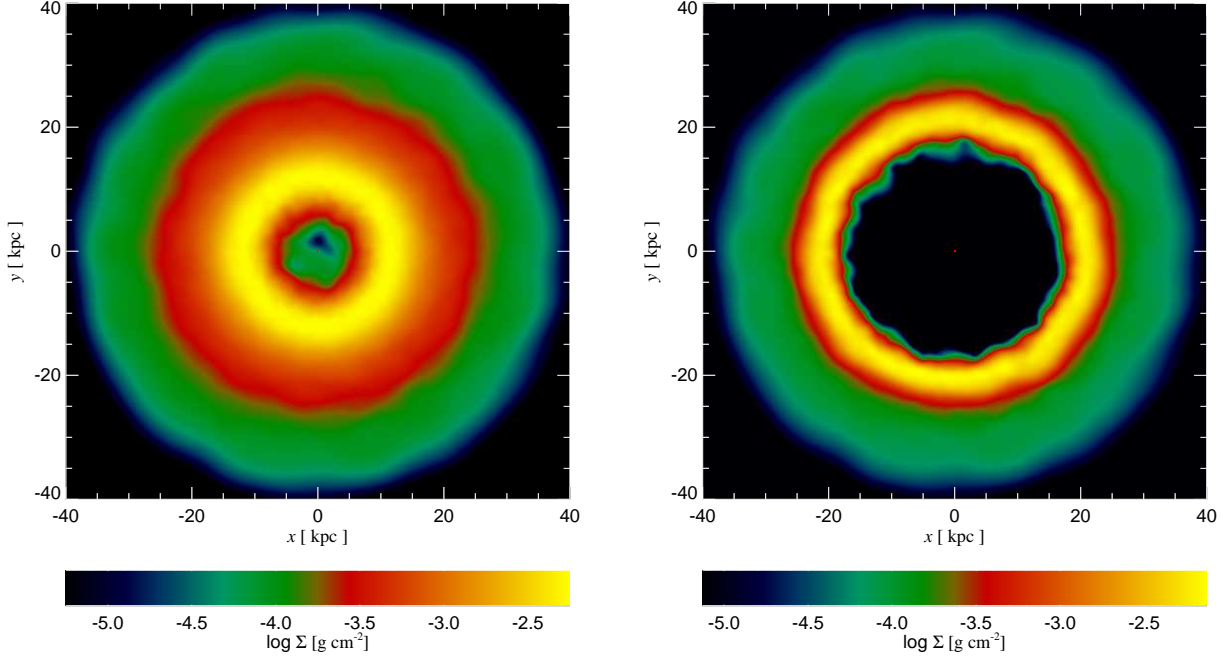


Figure 1. Typical results of the spherically symmetric tests. Left panel: shell collapsing on the $M_{\text{bh}} = 2 \times 10^8 M_{\odot}$ black hole (§2.3). Right panel: same shell but the black hole mass is $M_{\text{bh}} = 4 \times 10^8 M_{\odot}$, sufficient to drive the shell out (§2.4). Both snapshots are done at time $t = 70$ Myrs. See §2.1 for description of the figure.

tion of the shell after this point would require much greater numerical resolution and, more importantly, the physics of star formation.

The additional inward acceleration of the shell at $t \sim 40$ can be understood if one considers the self-gravity of the gas. We calculate the velocity dispersion corrected for the shell’s self-gravity:

$$\sigma_{\text{sh}}^2(R) = \frac{G}{2R} [M_{\text{DM}}(R) + M_{\text{sh}}] = (1 - f_{g0}) \sigma_0^2 + \frac{GM_{\text{sh}}}{2R}, \quad (7)$$

where $R = R_{\text{sh}}$. The second term increases for a constant M_{sh} and a decreasing R_{sh} . It is convenient to define a “running” value of the expected M_{σ} value based on the mean values of σ_{sh} and R_{sh} using equation 3. Further, we use the dimensionless variable m_{σ} :

$$m_{\sigma} = \frac{M_{\sigma}(R_{\text{sh}}, \sigma_{\text{sh}})}{M_{\sigma 0}} = \frac{f_g}{f_{g0}} \left(\frac{\sigma_{\text{sh}}}{\sigma_0} \right)^4, \quad (8)$$

where $M_{\sigma 0} = M_{\sigma}(R_0, \sigma_0)$ is the initial value of the M_{σ} mass as a function of the initial values of shell radius R_0 and velocity dispersion σ_0 , and f_g and f_{g0} is the current mass fraction of gas inside radius R . The function m_{σ} is plotted in Figure 3 with the dashed curve for the present simulation. It becomes immediately apparent that the SMBH will find it harder to retard the shell once the shell has fallen in sufficiently deep into the potential and the gas starts to dominate the gravitational potential. If SMBH mass is below the critical mass then a runaway radial contraction of the shell occurs in this simple model.

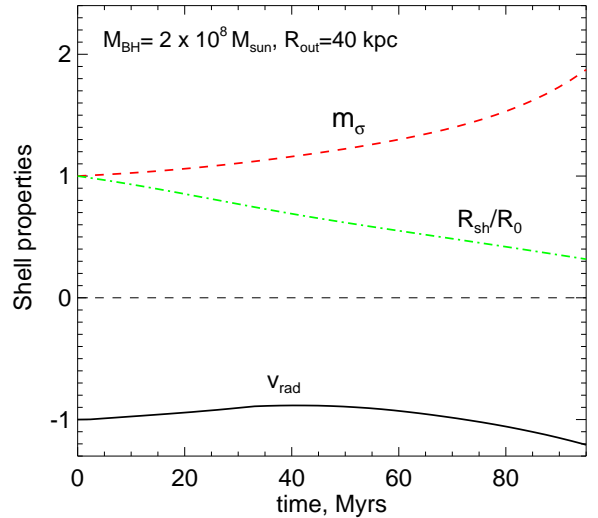


Figure 3. Mean radial velocity (solid) and radius (dash-dotted) of the gaseous shell as a function of time for $M_{\text{bh}} = 2 \times 10^8 M_{\odot}$. The dashed curve shows the expected dimensionless m_{σ} mass, as defined by the equation 8. The simulation is described in §2.3.

2.4 Initially infalling shell, $M_{\text{bh}} = 4 \times 10^8 M_{\odot}$

Figure 4 shows the result of exactly the same calculation but now with a SMBH mass twice as large, i.e., $M_{\text{bh}} = 4 \times 10^8 M_{\odot}$. The behaviour of the shell in this case is radically different. The average radius of the shell decreases only

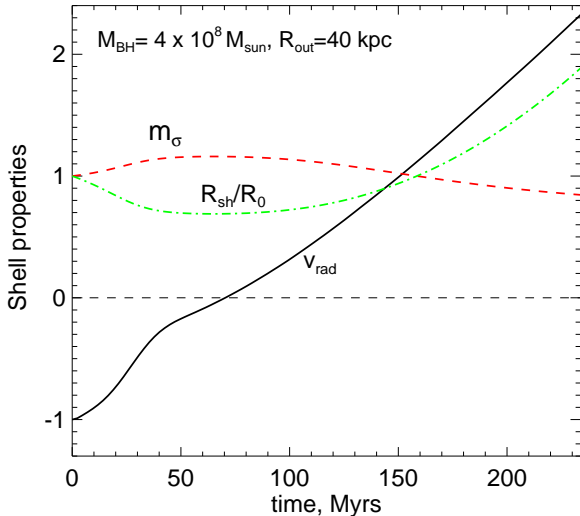


Figure 4. As in Figure 3 but now the black hole mass is a factor of two larger (§2.4). The gaseous shell is now completely expelled from the potential well to infinity.

during the first 40 Myrs, during which time the outermost layers of the shell continue to fall in. However, at $t \sim 40$ Myrs the shell briefly decelerates before quickly accelerating nearly linearly ($v_r \propto t$) out of the potential well.

It is worth noting how distinct the gas dynamics between the two cases illustrated in Figures 3 and 4 respectively. This may be somewhat surprising given that the SMBH mass and hence the outward acceleration differs between the cases only by a factor of two. However, the key difference is that in the first case the shell fell in far enough to become self-gravitating, with the self-gravity corrected σ increasing rapidly, increasing further the inward pull of gravity. This effect, missing in the analytical theory of King (2003, 2005), might actually increase the M_σ value above that given by equation 3.

Comparing the two initially infalling shell tests with those for an initially static shell (§2.2), we note that the critical black hole mass is increased by a factor of two or so to $M_\sigma \approx 3 \times 10^8 M_\odot$. This is natural as the shell needs to be accelerated to a positive velocity $v_r \gtrsim 1$ to be driven out of the potential, and that is comparable to the initial negative velocity of the infalling tests. The required outward acceleration should then be roughly doubled compared with the initially static tests. This shows that variations in the initial *radial* velocity of the shell are unlikely to change the critical black hole mass by more than a factor of a few.

2.5 Scale-free nature of fixed BH mass solutions

Equation 3 shows that the critical M_σ mass is independent of the initial location of the shell, R_0 , as long as the initial gas fraction $f_{g0} = M_{\text{gas}}(R_0)/M_{\text{tot}}(R_0)$ does not vary with radius. We now show that the same is true for time-dependent solutions. This can be seen from the equation of motion for gas in the one zone approximation, which is quite reasonable for a thin shell. We have

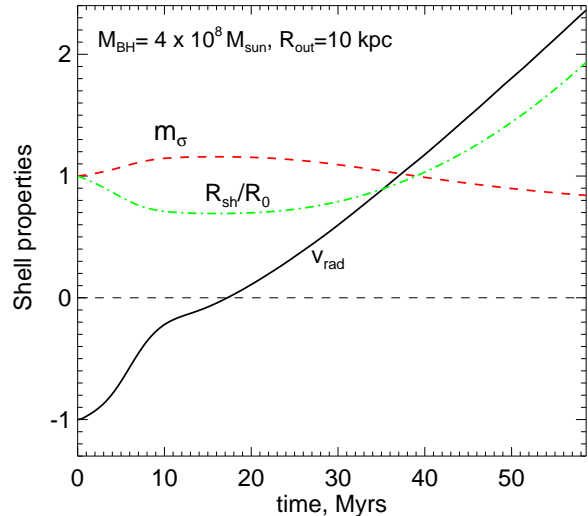


Figure 5. As in Figure 4, but now the initial shell radius is 10 kpc rather than 40 kpc. Note that the result is identical to Figure 4 save for the time axis shrinking by factor of 4. This confirms the scaling properties of the model discussed in §2.5.

$$M_{\text{sh}} \frac{dv_r}{dt} = \frac{L_{\text{Edd}}}{c} - \frac{G}{R^2} [M_{\text{DM}}(R) + M_{\text{sh}}] M_{\text{sh}}, \quad (9)$$

where $v_r = dR/dt$. Let us assume $R(t) = R_0 g(\xi)$, where $\xi = t/t_0$, $t_0 = R_0/\sigma$. Obviously, we require $g(0) = 1$. We can now re-write the above equation in this form:

$$\frac{R_0}{t_0^2} \frac{d^2 g}{d\xi^2} = \frac{L_{\text{Edd}}}{c M_{\text{sh}}} - \frac{2\sigma_0^2(1 - f_{g0})}{R_0 g} - \frac{G M_{\text{sh}}}{R_0^2 g^2}. \quad (10)$$

Only the dimensionless time variable ξ remains, implying a scale-free solution.

This conclusion is confirmed in Figure 5, which shows the result of a simulation identical to the one presented in Figure 4, except that the initial outer shell radius is $R_{\text{out}} = 10$ kpc rather than $R_{\text{out}} = 40$ kpc. The shell mass is also reduced by a factor of four to keep f_{g0} the same. It is readily apparent that the two figures are identical, with the only difference evident in the time coordinate.

This scale-free nature of the King (2003, 2005) model in the isothermal potential has interesting observational implications. The model predicts a slope and normalisation for the $M_{\text{bh}} - \sigma$ relation that is consistent with the observed ones, assuming only one free parameter f_{g0} fixed at the cosmological baryon fraction; however the overall scale of the system needs to be set by additional physics. King (2003, 2005) points out that this can be the requirement that the black hole outflow's cooling time is short compared with the local dynamical time, which fixes the ratio of the black hole to bulge mass to $\sim 10^{-3}$, in a good agreement with the observational data (e.g., Häring & Rix 2004).

In principle, other factors can be affecting the black hole to bulge mass relation, such as the finite extent of astrophysical potential wells, or the amount of angular momentum in the gas. We shall now consider the first issue in relation to the finite maximum growth rate of the black holes.

3 EDDINGTON RATE – LIMITED GROWTH MODELS

In §2 the black hole mass was assumed fixed for simplicity. In this section we allow the SMBH to grow at its Eddington accretion rate. In this case the SMBH mass increases by the factor of e in the Salpeter time,

$$t_{\text{Salp}} = \frac{M_{\text{bh}}}{\dot{M}_{\text{Edd}}} \approx 4.5 \times 10^7 \text{ yrs}, \quad (11)$$

where $\dot{M}_{\text{Edd}} = L_{\text{Edd}}/\epsilon c^2$ is the Eddington accretion rate, and the radiative efficiency ϵ is set to 0.1.

The initial value of the outer radius, R_{out} , defines another important time scale of the problem – the dynamical time,

$$t_{\text{dyn}} = \frac{R_{\text{out}}}{V_U}, \quad (12)$$

where $V_U = \sqrt{GM/R} \approx 208 \text{ km/sec}$ is the velocity unit for the potential.

As emphasised by Nayakshin et al. (2009b), there are two distinctly different regimes. If $t_{\text{Salp}} \ll t_{\text{dyn}}$, then the SMBH *can* grow arbitrarily quickly if provided with enough fuel. If there is a SMBH feeding-feedback link that can limit the SMBH mass, such as in the King (2003, 2005) model, the latter then grows to the appropriate M_σ mass and remains there. If $t_{\text{Salp}} \gg t_{\text{dyn}}$, then the SMBH is unable to grow sufficiently quickly to reach its maximum (i.e. M_σ), even if it is provided with ample fuel during the dynamical time of the system. We now present two simulations that explore these two regimes.

3.1 SMBH growth in a “large” bulge

The initial condition used in this test is same as in §2.3, except that the initial SMBH mass is smaller, $M_{\text{bh}} = 10^8 M_\odot$. As we found in §2.4 for this initial condition, the M_σ mass is about $M_0 = 3 \times 10^8 M_\odot$. The black hole thus needs to increase its mass by about a factor of 3 to drive the shell out. The dynamical time of the shell is $t_{\text{dyn}} \approx 200 \text{ Myrs}$, which gives the SMBH plenty of time to grow.

Figure 6 shows the mean radial velocity of gas (solid curve), the mean radius of the shell (dash-dotted), the self-gravity corrected velocity dispersion of the gas (dashed) and finally, the dotted curve shows the ratio of the black hole mass to the initial $M_\sigma = M_0$ mass.

The early phase of gas dynamics is quite similar to the underweight fixed mass case considered in §2.3. The shell is contracting and the gas velocity dispersion grows with time, increasing the M_σ value (see the dashed curve in the figure). However, the SMBH grows even faster. At around 90 Myrs the gas suddenly gets decelerated and then accelerated to positive velocity.

While this is as expected based on simple analytical expectations (Nayakshin et al. 2009b), the SMBH mass at the time when gas velocity becomes positive is about $1.3 \times 10^9 M_\odot$, about a factor of 4 higher than the initial configuration value, $M_\sigma = 3 \times 10^8 M_\odot$. At the same time, the shell radius is much smaller at that moment than the initial value, increasing the self-gravity corrected M_σ value by a factor of about 2.5 to $\sim 7.5 \times 10^8 M_\odot$. If our models included star formation and if a good fraction of gas

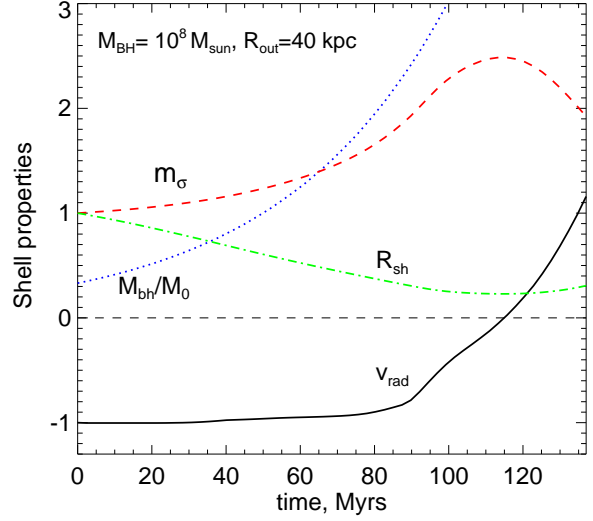


Figure 6. Gas mean velocity (solid), scaled mean radius (dot-dashed), scaled M_σ (dashed) and the ratio of the SMBH mass to the initial $M_\sigma = M_0 = 3 \times 10^8 M_\odot$ mass (dotted) for an Eddington limited simulation (§3.1). The initial SMBH mass is $10^8 M_\odot$, a third of the M_σ mass. However, due to rapid accretion the SMBH catches up with the growing (contracting) bulge and expels the gas when $M_{\text{bh}} \approx 1.3 \times 10^9 M_\odot$.

was turned into stars then the resulting bulge, assuming the stars remain bound as the gas is blown away, would satisfy the $M_{\text{bh}} - \sigma$ relation within a factor of two. However the bulge velocity dispersion would be higher than that of the underlying isothermal potential value.

3.2 SMBH growth in a “small” bulge

We now repeat the run of §3.1 but shrinking the shell’s outer radius by a factor of four to $R_{\text{out}} = 10 \text{ kpc}$ and increasing the SMBH’s initial mass to $M_{\text{bh}} = 2 \times 10^8 M_\odot$. This is about two thirds of the initial M_σ mass, and hence the black hole needs to increase in mass by only a small fraction to reverse the inflow of gas. However, as Figure 7 demonstrates, the black hole’s growth is too slow for this configuration of gas. As SMBH mass grows, so does the required m_σ mass, since the shell contracts. In fact, when the shell’s mass exceeds the local dark matter mass the shell becomes self-gravitating and the increase in m_σ accelerates, leaving no chance for the SMBH to catch up.

The results of these experiments confirm that the Salpeter time should be sufficiently short compared to the dynamical time of the system in order for the SMBH feedback to compensate for the shell contraction. However, if star formation had been included, removing some of the available gas and producing its own feedback, this requirement could be relaxed somewhat.

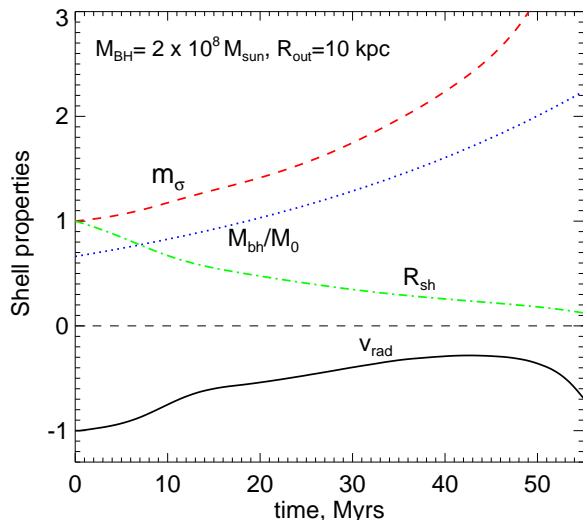


Figure 7. Similar to the simulation shown in Figure 6 but with a smaller initial radius of $R_{\text{out}} = 10$ kpc, and a larger initial SMBH mass of $2 \times 10^8 M_{\odot}$. Note that the feedback from the growing SMBH is unable to prevent the contraction of the shell in this simulation.

4 FEEDBACK ON GAS WITH ANGULAR MOMENTUM

So far we have neglected the angular momentum of the gas, instead looking at problems in which the motion of the shell is purely radial. However, we expect the gas to have non-zero angular momentum and this will be as important for the impact of the SMBH feedback, if not more so, than how the gas is distributed or what its thermodynamical properties are. If all the gas in the bulge possesses non-zero angular momentum with respect to the black hole, then its feeding must proceed through a disc. As efficiency of disc accretion is not well understood in the presence of star formation in massive cold discs (e.g., Goodman 2003; Nayakshin et al. 2007), the exact distribution of gas in the angular momentum space prior to disc formation is very important. Furthermore, on larger scales the angular momentum of gas determines the resulting scale of the galactic disc, and perhaps the bulge.

The parameter space of this problem is very large, and so we can only begin to scratch the surface of the problem here. We choose to study a case of the same initially spherical shell infalling with $v_r = -1$ at $t = 0$, $R_{\text{out}} = 40$ kpc (e.g., §2.3), but now rotating around the z -axis. In the spherical coordinates, in which $z = r \cos \theta$, $x = r \sin \theta \cos \phi$, $y = r \sin \theta \sin \phi$, the rotation law is given by

$$v_{\phi} = v_{\text{rot}} \sin \theta, \quad (13)$$

where v_{ϕ} is the ϕ -component of velocity, and $v_{\text{rot}} = 0.3$. Thus material near the pole rotates slowly while material near the equator ($z = 0$) rotates at the maximum for the test. We expect these tests to be geometrically more complicated than the spherical shell tests. Therefore, we significantly improve the resolution of these simulations by em-

ploying $N_{\text{SPH}} \approx 4 \times 10^5$ particles, i.e., by more than a factor of 10.

4.1 Gas dynamics without feedback

We begin by studying the dynamics of the gas in the absence of feedback from the black hole. Figure 8 shows two snapshots of the simulation viewed edge-on. We also show velocity vectors of the gas. In this figure and in all others showing velocity information, the normalisation of velocity vectors is not to unit velocity but to the largest velocity found in the snapshot. This is convenient as a subset of gas can have a velocity much larger than unity in the more complex cases considered below, and its velocity vectors then clutter the figures.

As expected, a gaseous disc forms with an outer radius of about $R \sim R_{\text{out}}/3 \sim 13$, appropriate for the rotation velocity equal to about a third of the circular velocity in the isothermal potential. The inner radius of the disc goes all the way to our inner boundary of the simulation domain, $R = 0.5$ kpc, since the regions close to the polar axis have small angular momentum. By late times about 4% of the gas disappears inside the inner boundary. The disc undergoes radial oscillations for many orbits before the gas settles on circular orbits. Signatures of these oscillations can be observed in the right panel of Figure 8, where the disc vertical structure is not completely relaxed. In particular, one can see some low density regions having a small positive radial velocity in the corners of the Figure.

Due to the high gas temperature selected for the simulations, $T = 3 \times 10^5$ K, the vertical pressure scale-height of the final disc is relatively large, $H/R \sim 0.3$. Realistic discs are expected to be cooler, and thus could be geometrically thinner and denser. However star formation in these discs and especially feedback due to star formation may make such discs vertically more extended than one would get from simple estimates based on their temperature only. In any case, our deliberate choice of a rather geometrically thick disc implies that our main conclusions on the role of angular momentum, to be drawn below, can only be strengthened if discs are thinner and denser.

4.2 Feedback and disc formation

We now turn to simulations with black hole winds. In order to isolate the main effects in the interplay between the feedback and angular momentum, we consider the simplest case of a constant and isotropic feedback. The momentum flux from the black hole is fixed at the value appropriate for a black hole mass of $M_{\text{bh}} = 2 \times 10^8 M_{\odot}$, as in §2.3.

Figure 9 shows two snapshots from the simulation. The left panel of Figure 9 demonstrates a rather obvious point – that inflow is slower in the presence of feedback than in its absence (Figure 8); in fact, the inner region is devoid of gas. As in the spherically symmetric feedback cases, a shell is formed. The shell is not spherical. The equatorial regions are held back by the centrifugal force more than the polar regions. Whilst this is occurring, gas also starts to accumulate in the midplane, just like it does when there is no feedback. Because there is a competition between feedback and centrifugal forces on the one hand, and gravity of the

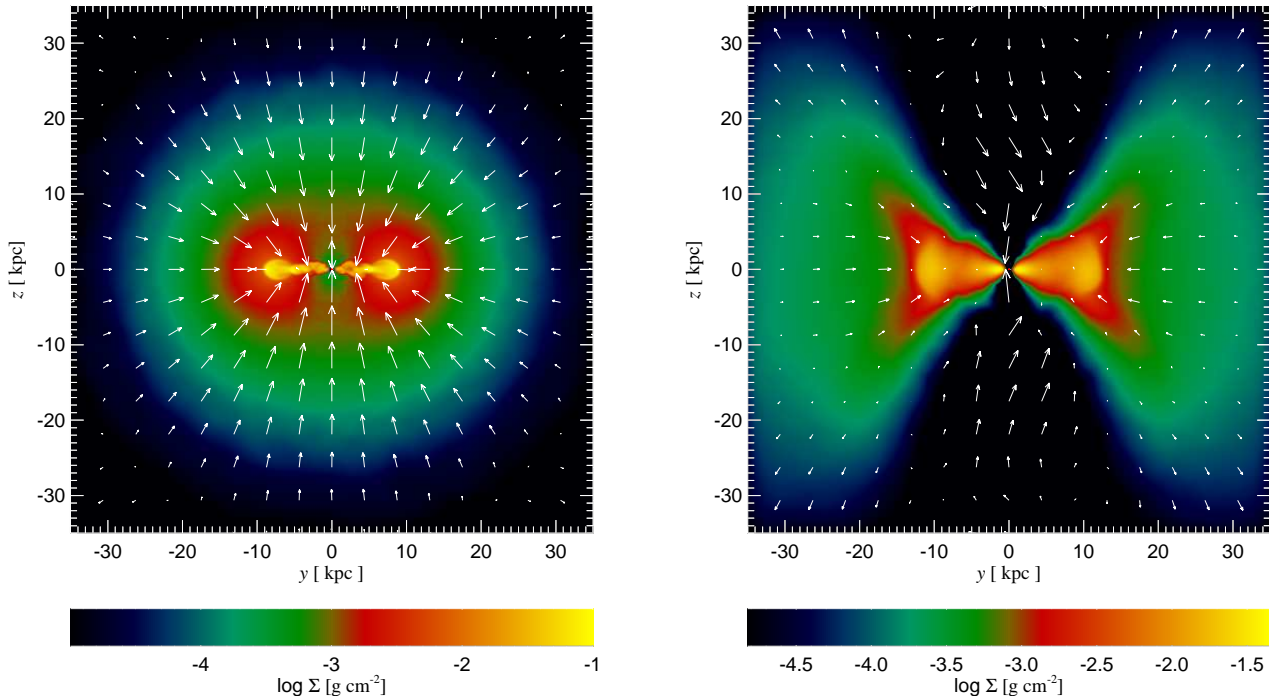


Figure 8. Column density in the edge-on projection of the collapsing shell for simulation without feedback. Left: time $t = 95$ Myrs. Right: $t = 230$ Myrs. The final relaxed disc is hydrostatically supported at $H/R \sim 0.3$. Note the high density inner disc. About 4% of the shell has been accreted by the inner boundary at $R = 0.5$ kpc.

other, a ring – rather than a disc – is seen to form just beyond the shock front in the right panel of Figure 9. Also note that the cavity is not perfectly azimuthally symmetric at later times (right panel), due to the development of a combination of instabilities and the self-gravity of the gas.

Figure 10 shows two snapshots at a later time. A bipolar initially bubble-like structure develops around but not exactly on the symmetry axis. The bubble quickly bursts and a cavity is opened along the symmetry axis. In that region some gas is driven sideways, by the centrifugal force, and some to infinity by the black hole wind. At later times the central region $R \lesssim 10 - 15$ is devoid of gas except for the black hole wind. Gas on the interface between the void with the higher density gas is continuously stripped away, feeding the (secondary) outflow.

The centrifugal force rarefies the region of the shell near the poles, and the black hole winds then evacuate that region by pushing the gas away. In the equatorial plane, on the other hand, the disc becomes too dense for the black hole feedback to have much of an effect. The disc manages to shadow its interior from the black hole influence.

Analysing the net effect of the finite angular momentum of the shell on the feedback-shell interaction, we note that the polar regions can now be expelled more easily. If these regions are to ultimately provide the SMBH with fuel then this would reduce the required M_σ mass. However, it is now much more difficult for the SMBH to affect the self-shielding disc. The mean density in the disc is $\sim R/H$ times higher than the density for the same mass spread in a spherical volume. If it is the disc that provides the SMBH with fuel, then one would predict a value for the M_σ mass higher than

the equation 3 by at least the factor of R/H . Indeed, in case of isotropic feedback, the fraction of SMBH wind intercepted by the disc is $\sim H/R$. If feedback is anisotropic and beamed away from the disc, as would seem natural for a “grand design” disc, i.e., one extending from galaxy scales of kpc to sub-pc scales, then there is a further inefficiency in feedback delivery to the disc. This appears to contradict the recent observations of “pseudo bulges”, e.g. bulges that are disc or bar-like. The SMBH masses in such bulges appear to be smaller rather than larger than those in classical bulges at the same velocity dispersion (Hu 2009).

In fact it is hard to see why there would exist any $M_{\text{bh}} - \sigma$ relation at all if SMBH were fed by large scale discs that are immune to the SMBH feedback.

5 COLLIMATED FEEDBACK

There are good reasons to believe that feedback may be collimated rather than isotropic. Unlike stars that radiate due to internal energy sources, black holes need a continuous fuel supply in the form of accreting gas. Thus there must be regions where feedback is relatively inefficient and net inflow dominates. Most likely such inflow takes the form of a standard accretion disc (Shakura & Sunyaev 1973) on scales of mpc and less. The outflow is then probably stronger along the axis of symmetry of the disc. In addition, the putative molecular torus is probably quite a massive and geometrically thick structure (e.g., Krolik & Begelman 1988) that may restrict the black hole outflow to the direction perpendicular to the midplane of the torus (if one can be defined).

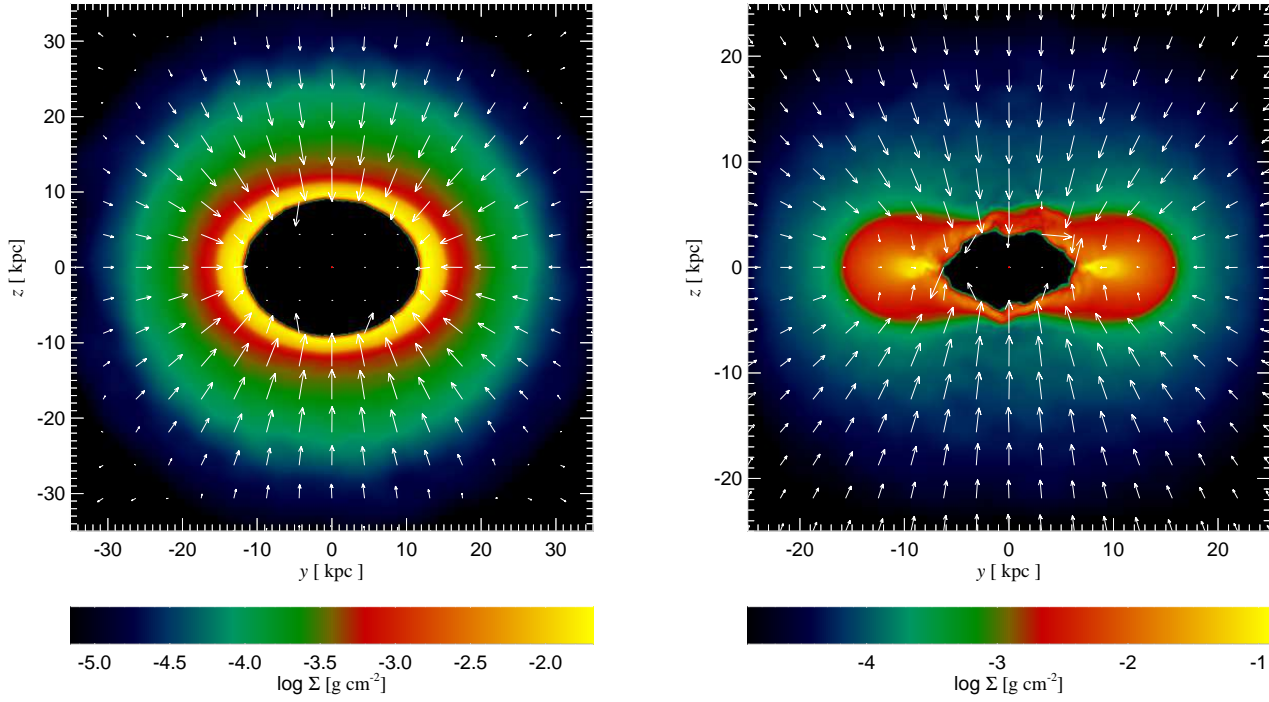


Figure 9. As in Figure 8 but with feedback, and at times $t = 95$ Myrs (left panel) and $t = 130$ Myrs (right panel).

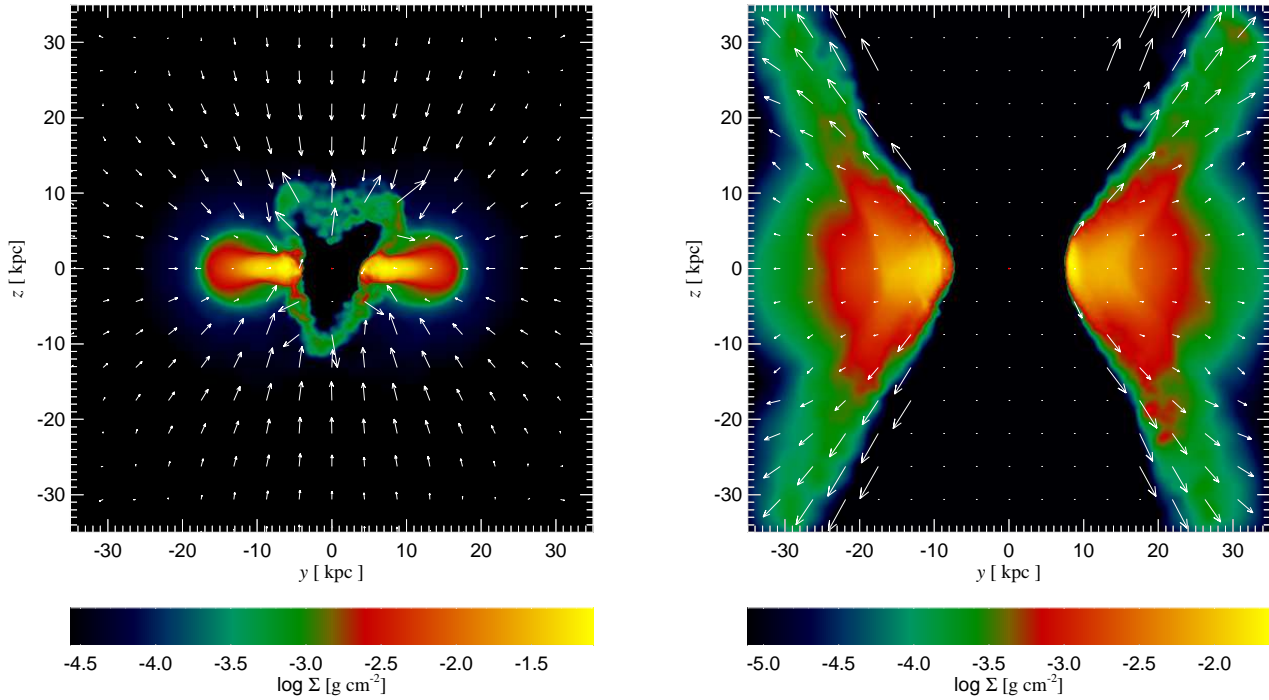


Figure 10. As in Figure 9 but for later times. Left: time $t = 145$ Myrs. Right: $t = 275$ Myrs.

Note that the inner accretion flow does not have to be co-aligned with the torus, especially if the black hole is rapidly spinning (King et al. 2005). If direction of the flow fluctuates rapidly compared with the time scales of bulge formation, $\sim 10^8$ years, then we arrive at possibly quite a complex picture of black hole outflows – non-stationary, non-spherical and with a fluctuating direction.

How is the momentum feedback picture developed for the spherical model (King 2003, 2005) modified when these collimation effects are taken into account? The answer is probably very complicated and depends on the setting/environment. Here we present simulations for two relatively simple situations, designed to motivate further discussion rather than give final answers.

5.1 Outflow misaligned with the disc

Our first simulation uses a fixed black hole mass $M_{\text{bh}} = 2 \times 10^8 M_{\odot}$ for simplicity, and the same rotating shell initial condition used in the simulations presented in §4.2. However, rather than assuming isotropic feedback, the black hole feedback is now uniformly distributed within the angle $0.7 \leq |\cos \theta'| \leq 1$ around the symmetry axis z' (see below). Note that within this conical region the momentum flux density carried by the black hole wind is $1/0.3 \approx 3$ times higher than in the isotropic case studied in §4.2.

We anticipate that the effect of collimated feedback when the axis of symmetry coincides with the z -axis should be qualitatively similar to the effect of isotropic feedback on gas with non-zero angular momentum, of the kind presented in (§4.2). Therefore we consider a less trivial case in which the direction of the axis of symmetry of the outflow, z' , is inclined by angle $\pi/4$ from the z -axis defined by the direction of the angular momentum vector of the shell. For convenience of presentation, we choose the angular momentum vector of the shell and the outflow symmetry axis to lie in the $z - y$ plane.

Figure 11 shows angle-slice projections of the gas surface density at times $t = 23$ Myrs (left panel) and $t = 59$ Myrs (right panel). The projections are done along the x -axis, as before. In this projection both the disc axis of rotation (z -axis) and the outflow axis of symmetry are in the plane of the figure. It is apparent from Figure 11 that the outflow drives strong non-spherically symmetric motions in the infalling shell, sending gas on different non-circular orbits inclined to the z -axis at various angles.

The evolution of the shell is different from anything seen in the previous tests. Initially (see the right panel of the figure) regions of the shell directly exposed to the feedback are compressed into a thin shell, which is slowly driven outwards. However, because the shell is rotating, gas that was not previously exposed to feedback continuously replenishes the outflow's cone, and most of the shell eventually collapses inwards rather than being driven outwards, as is seen in the right panel of Figure 11.

At the same time, the segments of the shell not exposed to feedback at all – regions along the diagonal line from the left upper corner to the right lower corner of the figure – approach the black hole initially almost freely falling (the right panel). At later times their radial motion is stopped by the centrifugal force. Some parts of the gas then appears to be pushed into the feedback cone by the ram pressure of

the continuous inflow. These parts are blown away into the outflow.

This geometrically complicated interplay of feedback and rotation results in a very strongly warped rotating structure visible in Figure 12 at time $t = 100$ Myrs. Here we show two projections, one along the x -axis (left panel) and the other along the z -axis (right panel) for clarity. Note the circularising motions of gas at larger radii, settling into the disc. These regions of the disc are shielded from the black hole outflow by the inner disc regions. The inner disc regions are highly disturbed, however, with tangential, outflowing and inflowing motions present (see the central part of the right panel of Figure 12).

Figure 13 shows two later stages in the evolution of the system. The left panel of the figure is for time $t = 160$ Myrs, whereas the right panel shows $t = 400$ Myrs. Apparently the feedback is eventually able to clear the directions in which it is operating to enforce a strong outflow in those directions. In short, parts of the disc perpendicular to the outflow do survive, whereas the less fortunate parts, in the path of the black hole wind, are blown away by the wind. This occurs on roughly the dynamical time of the original shell ($R_{\text{out}}/\sigma \approx 190$ Myrs). However this is probably a function of the assumed disc temperature. A cooler and thicker disc could be more difficult to affect; more simulations of this are needed in the future.

The resulting “truce” between the black hole outflow and the inertia of the disc is not an easy or natural one. The disc is warped and is still an evolving structure, with gas orbits in the inner part being nearly circular while those in the outer parts are more eccentric. The outflow also has a faster and slower parts, with the denser regions moving more slowly. Not all parts of the outflow reach escape velocities before becoming shielded, and some falls back along directions not exposed to the black hole outflow.

Comparing this simulation to the one with isotropic black hole wind (§4.2), it is apparent that collimated feedback leads the separation of the gas into disc and outflow regions to occur much later in time. Furthermore, this separation is nowhere near as clear cut as in §4.2. In addition, while no gas was able to reach the accretion radius of $R_{\text{acc}} = 0.5$ kpc in the spherically symmetric feedback simulation, the misaligned feedback run resulted in about 1% of gas crossing the inner boundary. This value is still significantly less than the 4% of gas accreted in the control simulation with no feedback (§4.1).

5.2 Outflow with a rotating axis of symmetry

The final simulation that we present here has a set-up similar to the previous simulation of misaligned collimated feedback, except in this case the feedback axis is rotating around the x -axis according to:

$$\theta_{\text{out}} = \Omega_{\text{out}}^{-1} t, \quad (14)$$

where $\Omega_{\text{out}}^{-1} = 30$ Myrs (the simulation in §5.1 corresponds to a constant $\theta_{\text{out}} = \pi/4$). Thus the outflow axis becomes perpendicular to its original position in 15 Myrs. Realistically, we might expect changes in the direction of black hole rotation to occur on even shorter timescales (King & Pringle 2006), and so this simulation is probably still less complex than realistic bulges.

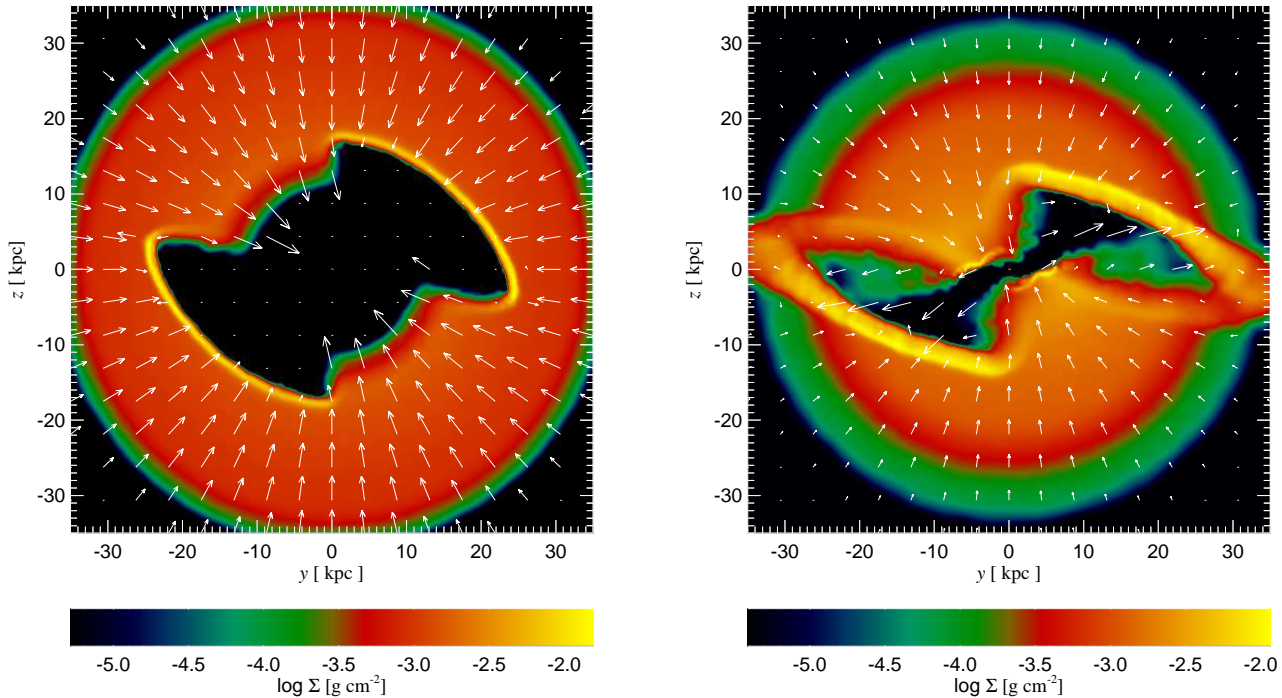


Figure 11. Angle-slice projected densities for the misaligned simulation at times $t = 23$ (left panel) and $t = 59$ (right panel) Myrs.

Figure 14 shows the angle-slice projections of the simulation at times $t = 47$ (left panel) and $t = 83$ (right panel) Myrs. Figure 15 shows the same but at times $t = 120$ (left panel) and $t = 165$ (right panel). There are certain similarities in gas dynamics between the present simulation and that with the misaligned collimated outflow (§5), but there are also significant differences. One similarity is the presence of gas inflow along directions not presently exposed to the black hole outflow, and outflow along some directions. However, there does not appear to be a settled structure in this case at all. Very strong velocity gradients and transient shocks occur in the present simulation. Such time dependent shocks may be efficient drivers of gas turbulence.

6 FEEDBACK AND TURBULENCE

Figure 16 shows the radial velocity structure for the SPH particles in the isotropic feedback simulation in which the shell had some angular momentum at a time of $t = 236$ Myrs. As we remarked in §4.2, the feedback and the disc achieve a natural division of the available space on the spheres of influence. Along the directions close to the pole, feedback dominates. In the midplane, most of the disc particles are shielded by the inner edge of the disc. The intermediate region is taken up by the wind driven off from the inner edge of the disc by the feedback. These features are clearly observable in Figure 16 in terms of the radial velocity component.

We now consider the radial velocity plots for the simulation with a misaligned (stationary axis) outflow, §5.1. Figure 17 shows that initially the radial velocity distribution is quite complex, but this settles into the warped disc – outflow

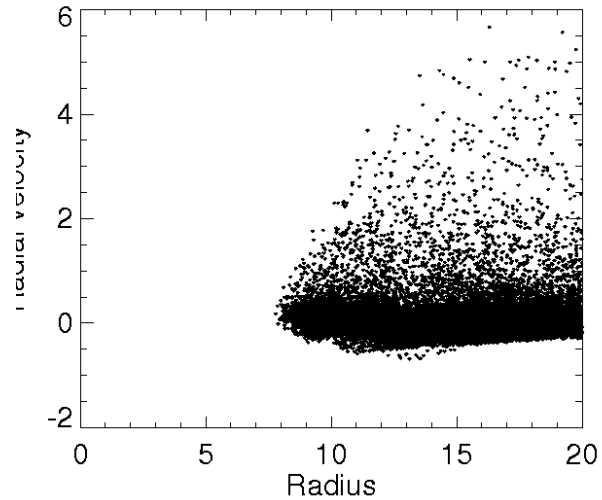


Figure 16. Radial velocity of SPH particles versus their radial distance to the black hole for the isotropic feedback simulation with rotation, see §4.2 and figure 10. The dominant feature is rotationally supported disc, and the points above it are the SPH particles in the outflow.

structure fairly quickly already by the time $t = 59$ (lower panel) of the figure. With time this configuration evolves into a progressively more quasi-stationary state.

In contrast, when the outflow is rotating (Figure 18), no clear cut steady state is reached. The radial velocity pattern

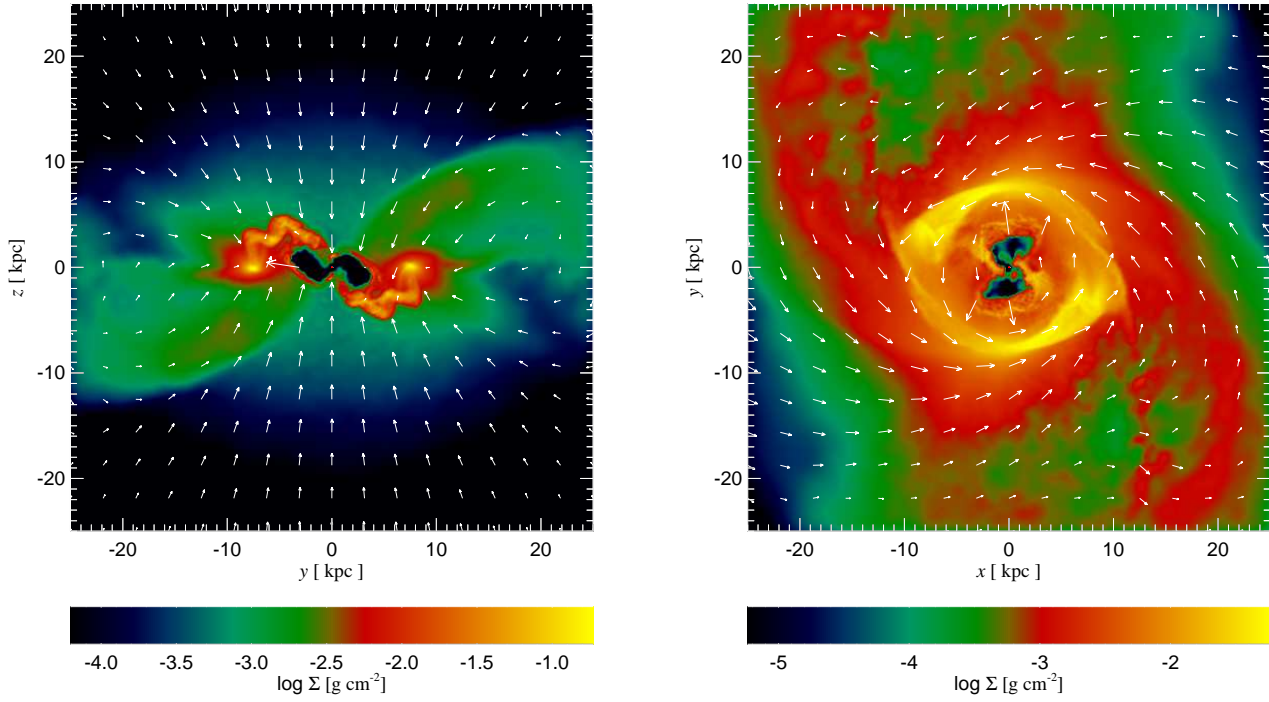


Figure 12. Left panel – As in Figure 11 but for time $t = 105$ Myrs; note that the scale has changed. Right panel – same time but the density projection is along the z -axis.

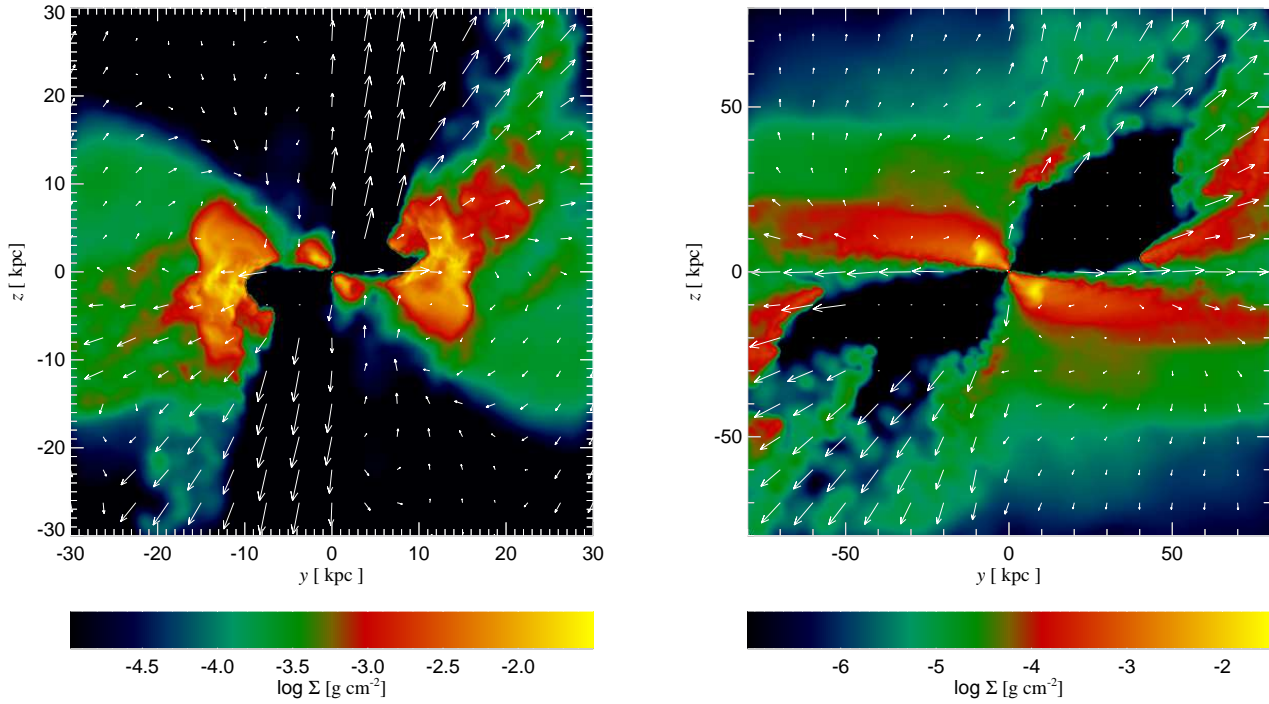


Figure 13. As in Figure 11 but for later times: $t = 160$ Myrs and $t = 400$ Myrs for the left and the right panels respectively. The outflow eventually evacuates the directions along which it acts; only the inclined part of the disc that is shielded from the feedback survives to late times.

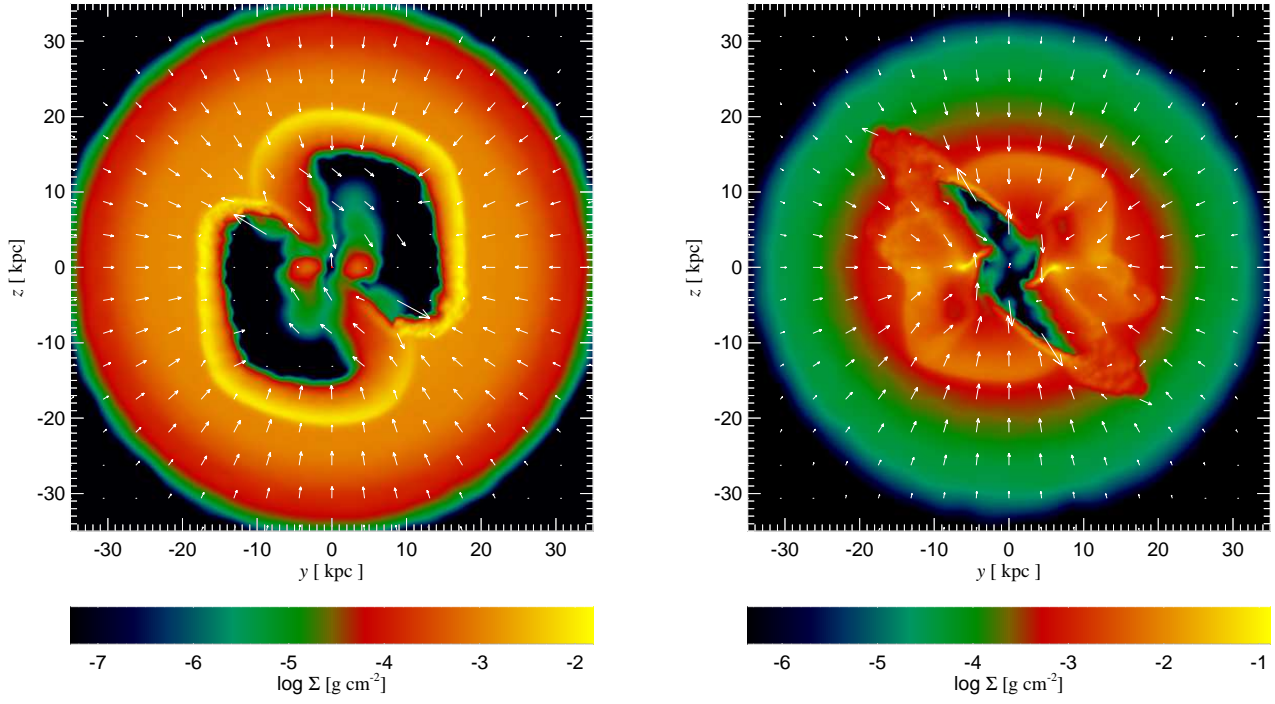


Figure 14. Simulations with a rotating “jet” outflow. Left panel is for time $t = 47$ Myrs, and right is for $t = 83$ Myrs.

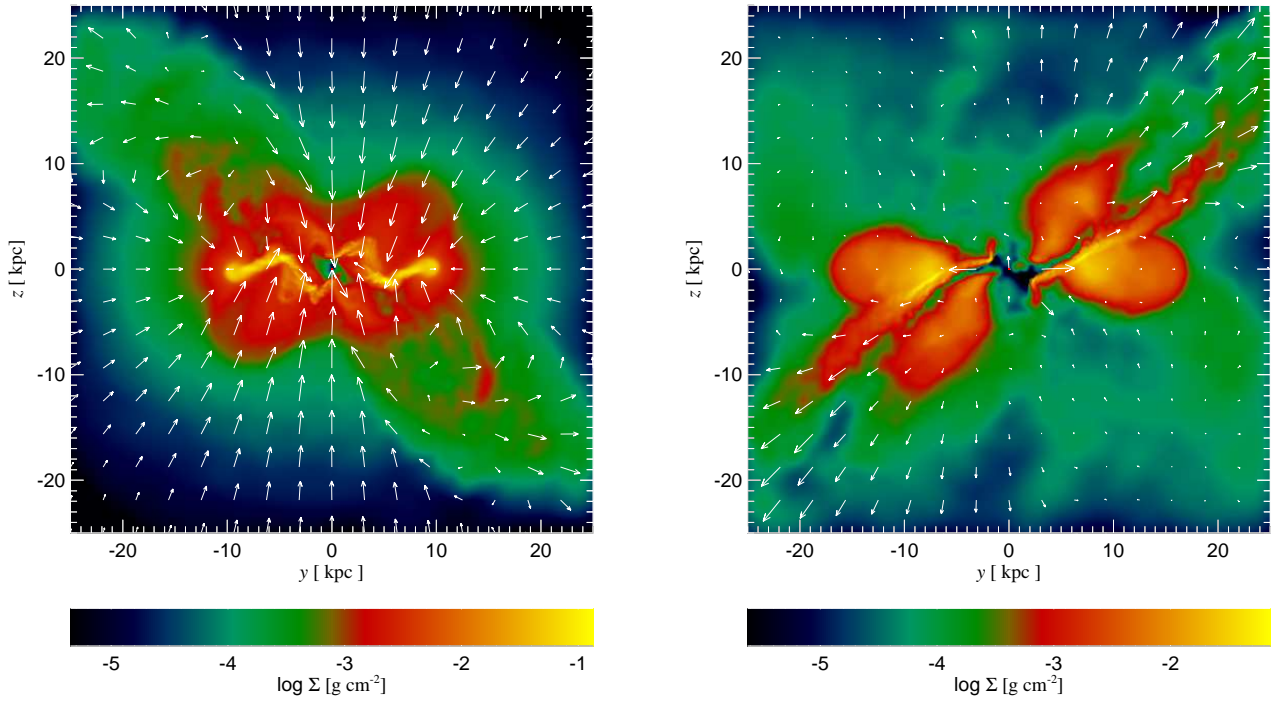


Figure 15. Same as Figure 14 but for later times: $t = 120$ Myrs and $t = 165$ Myrs for the left and the right panels, respectively.

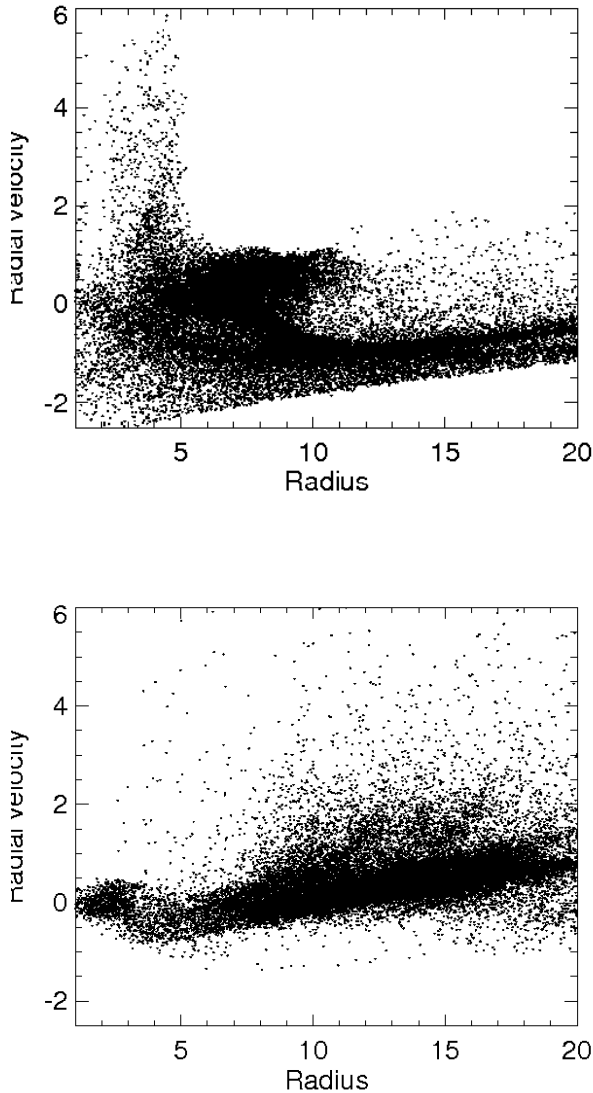


Figure 17. Same as Figure 16 but for simulation with an inclined collimated outflow (§5.1) at two different times, $t = 23$ (upper panel) and $t = 59$ (lower panel) Myrs. See Figure 11 for the edge-on view of the simulation.

keeps evolving on time scales comparable to the rotation period of the jet at relatively late times. One observes development of occasional transient shocks such as the vertical feature in the bottom panel of Figure 18. The SMBH feedback thus provides momentum input into complicated differential gas motions, probably pumping turbulence in the bulge.

We believe this is in fact another way in which the SMBH can be affecting its host galaxy. The current consensus in the field of star formation points to the key role of turbulence in providing support against gravitational collapse of gas on large scales while allowing star formation to proceed on smaller scales in dense filaments (for recent reviews see Mac Low & Klessen 2004; McKee & Ostriker 2007). As turbulent motions are not equivalent to an isotropic pressure

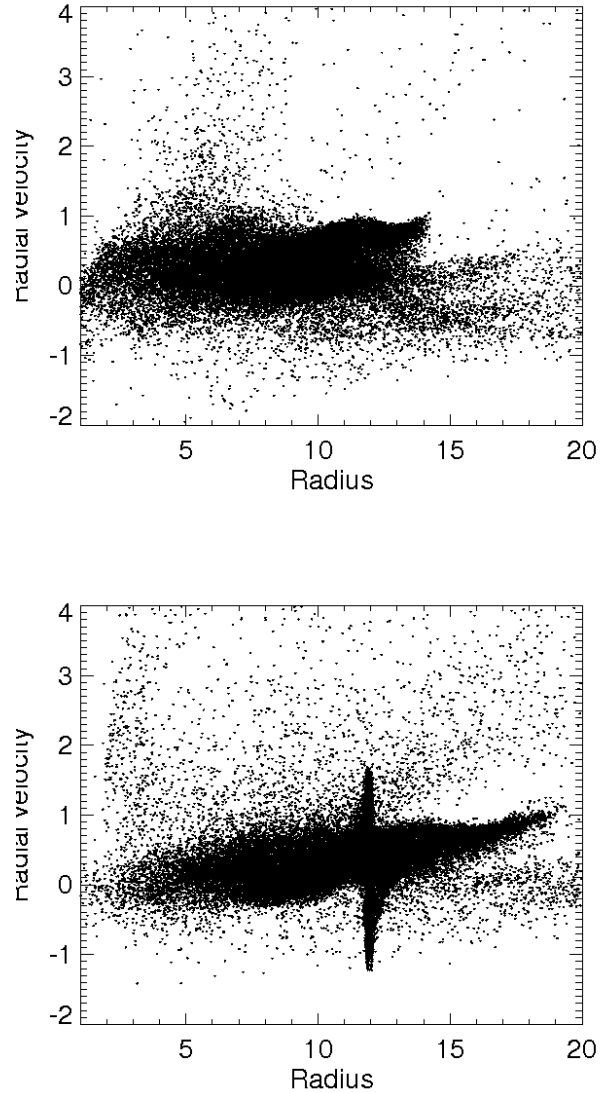


Figure 18. Same as Figure 17 but for simulation with a rotating collimated outflow (§5.2) at two different times, $t = 141$ (upper panel) and $t = 165$ (lower panel) Myrs. The vertical feature in the lower panel is a strong transient shock.

support (Dobbs et al. 2005), the main effect of the turbulence is to delay or slow down star formation. While future higher resolution studies are needed to confirm the point, it appears intuitively clear that AGN-driven turbulence in the bulge can also hinder star formation in its host bulge. In this case the host is affected by the SMBH feedback in two ways: not only the gas is being blown away but also the fraction of gas turned into stars is reduced.

7 DISCUSSION

7.1 Spherically symmetric models: successful feedback

Spherically symmetric models can be considered a success to a certain degree since earlier analytical work is confirmed by the more detailed calculations here. First of all, the analytical estimate of the critical M_σ mass obtained by King (2003, 2005) agrees well with our numerical simulations, especially for an initially static shell (see §2.2). If the shell is already falling in, then the added inwardly directed inertia of the shell raises the M_σ mass by a factor of a few at most (§2.3 and §2.4).

The complications arising from a finite system size were recently pointed out by Nayakshin et al. (2009b) who noted that dynamical time in the bulge, R_b/σ , where R_b is the scale radius of the bulge, plays a key role in what happens. Black holes growing at the Eddington rate, \dot{M}_{Edd} , e -fold their mass on the Salpeter time, $t_S = M_{\text{BH}}/\dot{M}_{\text{Edd}} \approx 4.5 \times 10^7$. Observationally,

$$t_{\text{dyn}} = \frac{R_b}{\sigma} = 17 \text{ Myrs} \left[\frac{\sigma}{150 \text{ km s}^{-1}} \right]^{2.1}. \quad (15)$$

Thus “large” bulges, $\sigma \gtrsim 200 \text{ km s}^{-1}$, have dynamical times comparable or larger than t_S . Under the assumption that the duration of the black hole feeding event is comparable to the dynamic time of the bulge then, these “large” bulges allow sufficient time for their SMBH to grow significantly. These bulges would then have “fully grown” black holes saturated at their M_σ mass. On the other hand, lower mass bulges with velocity dispersions of $\sigma \lesssim 100 \text{ km s}^{-1}$ would evolve too rapidly for their SMBHs to “catch up”. Therefore feedback from these SMBH would be overpowered by the inflow of gas from the bulge. The central regions of these lower mass bulges could be sites of copious star formation, leading to the birth of nuclear star clusters. The latter then reach their $M_{\sigma*}$ masses (see Nayakshin et al. 2009b), replacing the SMBH black holes as the dominant objects in the bulges.

Our simulations (§3) confirm this effect. The numerical experiment in §3.1 has shown that black hole immersed in a 40 kpc bulge is able to grow enough to expel the gaseous shell when started from initial mass of $M_{\text{bh}} = 10^8 M_\odot$ (Fig 6). At the same time, a black hole that is initially twice as massive in a 10 kpc bulge is unable to expel the shell (§3.2, Fig. 7) that is less massive than that in §3.1.

One complication not considered by analytical models yet is that if the mass fraction of gas is significant, i.e. larger than the universal cosmological fraction of $f_g \approx 0.16$, then the self-gravity of the gas can dominate the potential. The weight argument of course applies to self-gravitating shells as well, and they too can be unbound by a sufficiently strong black hole wind (e.g., see Figure 6). However in this case our models are inconclusive as they do not include star formation. When gas is blown away, the velocity dispersion of the self-gravitating shell should decrease. A detailed calculation including star formation is needed to establish whether or not the black hole in the remaining bulge follows the $M - \sigma$ relation.

7.2 Spherically symmetric models: inconsistent SMBH feeding

There are at least two major worries about the general usefulness of spherically symmetric models. Large scale cosmological simulations usually produce very complicated gas density and velocity flows onto the centres of dark matter halos (e.g., Kereš et al. 2005) and so it is not clear whether or not such spherically symmetric flows ever take place.

There is also a conceptual difficulty with the spherically symmetric models. In a self-consistent model, where black hole feedback is linked to the accretion of gas onto the hole, one cannot have accretion and outflow at the same time. Yet both are needed. We need accretion to grow and power the SMBH, but we also need outflow to eventually curtail the SMBH growth and expel the gas from the galaxy.

Having accretion before, e.g., while the SMBH has not reached the M_σ mass, and outflow later, after it has done so, is not a comfortable option. Indeed, to change inflow to outflow for most of the gas in a bulge, we require momentum input of

$$P \sim M_{\text{gas}} v_{\text{esc}} \sim M_{\text{bulge}} \sigma, \quad (16)$$

where M_{gas} is the mass of the gas which we assumed to be of order the bulge mass, M_{bulge} , and the escape velocity $v_{\text{esc}} \sim \sigma$. The minimum amount of mass that the black hole needs to accrete to produce this much momentum outflow is

$$\Delta M_{\text{min}} = \frac{P}{\epsilon c}. \quad (17)$$

For fiducial numbers $\sigma = 150 \text{ km/sec}$ and $\epsilon = 0.1$, we have

$$\Delta M_{\text{min}} = 0.005 M_{\text{bulge}}, \quad (18)$$

which is comparable to the observed M_{bh} masses for most bulges (Häring & Rix 2004). Now, if this gaseous mass is accumulated somewhere near the SMBH, e.g., in a disc that is immune to the feedback so that it can power the SMBH, then the question is why could this mass not be much higher or much lower?

In other words, if SMBH feeding is local to a small scale region (for example, inside the SMBH influence radius, which is typically between a pc and a few tens of pc), where enough material is stored to feed SMBH while most gas is driven away, the casual link between feedback and accretion is broken, and there does not appear a reason to have an $M_{\text{bh}} - \sigma$ relation. Thus spherically symmetric models, while providing excellent fits to the observed relations, do not naturally explain how the SMBH gets its fuel, or how it knows to stop growing once the many kpc scale shell starts to be blown away.

7.3 Non-spherical models: clear mode for feeding but not feedback

The second type of simulations that we considered here do not have spherical symmetry for one or more reasons. SMBH feeding in these models can be achieved (1) by features denser than the mean, i.e., discs or filaments, or (2) through regions not exposed to feedback at all. In the former case, if the SMBH-feeding gas has a column density (as seen from the black hole) much higher than the mean for the bulge, then it is only weakly affected by the momentum feedback.

In both of these cases there can be inflow to feed the SMBH and outflow to expel most of the gas in the bulge simultaneously. However, if these dense features feed the SMBH despite it producing feedback at the maximum rate, then it is not clear why there should be a feedback mediated SMBH – galaxy link.

This problem is already apparent in the simplest non-spherical case – the simulation of a rotating initially spherical shell of gas (§4.2). In that simulation gas separates out in two well defined regions – the polar region where black hole outflow dominates and the disc midplane where gas is shielded from the black hole outflow by the inner edge of the disc. The edge of the disc is slowly “evaporating” into an outflow. The rest of the disc is hardly affected, and the orbits there are nearly circular.

We have also set a numerical experiment in §5.1 where feedback outflow is confined to a broad cone misaligned with the rotation axis of the shell. The shell initial condition was identical to that explored in §4.2. We found, not surprisingly, that the resulting pattern of gas dynamics is even more complex than that of an isotropic feedback with a rotating shell. The inflow persists along directions in which black hole winds are not emitted, and the outflow prevails inside the feedback cone. The collimated rotating black hole outflow (§5.2) is even more complex geometrically, with black hole feedback probably driving turbulence into bulge gas.

7.4 Shortcomings and comparison to other numerical work

There is a substantial body of work on numerical simulations of SMBH feedback in cosmological simulations, e.g., Springel et al. (2005); Di Matteo et al. (2005); Sijacki et al. (2007). This paper complements this work. While addressing similar issues, the scales involved in studying SMBH feedback in a cosmological context are very different. Cosmological simulations have clear strengths – they naturally account for hierarchical build-up of galaxies assuming realistic initial conditions and they include recipes for physical processes that we expect to be important for galaxy formation such as cooling, star formation and feedback. Therefore they can provide a powerful tool with which to explore SMBH feedback. In comparison, our simulations are more modest in terms of the number of physical processes studied, making use of idealised initial conditions in static analytical potentials.

On the other hand, the all-inclusive nature of cosmological simulations mean that “individual” processes, such as black hole accretion and feedback, cannot be modelled in sufficient physical detail and require sub-grid physical models to be assumed. As far as we are aware, all the current cosmological simulations rely on Bondi & Hoyle (1944); Bondi (1952) formulation for accretion of gas. The latter formulation is physically inconsistent if accreting gas has angular momentum as gas simply cannot reach the SMBH due to the centrifugal barrier. Furthermore, at least the “quasar” mode of feedback is done in a very sketchy manner, with a fixed fraction of energy released by the quasar passed to the SMBH neighbour particles. The right fraction is found a posteriori to fit the observed $M_{\text{bh}} - \sigma$ relation and other observational constraints.

Therefore, modest “small scale” simulations such as

ours, especially when extended to include more physics and to reach in as close as possible to the SMBH may offer another important route to solving the mystery of SMBH and galaxy growth. Ideally, the small scale and cosmological simulations should be merged to some degree in the future to allow as self-consistent a study of SMBH feedback as possible.

8 CONCLUSIONS

Our main conclusions are

- Predictions of spherically symmetric models with black hole feedback tied to Eddington limit luminosity as in the models of King (2003, 2005) are confirmed numerically. Self-gravity of the gas complicates evolution of the system, and a self-consistent treatment of star formation and its feedback is necessary for further progress.
- As suggested earlier based on analytical arguments, it is the dynamical time in the bulge, R_b/σ , that determines whether or not the SMBH can reach its limiting M_σ value. Central regions of smaller bulges, where the dynamical time is observed to be shorter than the Salpeter time, could be smothered with infalling gas despite the SMBH feedback. This process may be the origin of the nuclear star clusters in “smaller” galaxies.
- A net angular momentum in the shell is essential in determining the fate of the shell and the SMBH feeding. There is no well defined M_σ mass in that case since the momentum thrust required is different in different directions. Gas near the symmetry axis is blown out easier than in the spherically symmetric case, whereas gas settled into a disc requires $\sim R/H$ more thrust than in the latter case.
- If the SMBH is fed through a several kpc scale disc, the SMBH mass would have to be $\sim R/H$ larger than in the spherical case to expel the feedback-resistant self-shielding disc. This directly contradicts the recent observations of Hu (2009) that show that pseudo-bulges have lighter SMBHs than their classical counter-parts. This may imply that black holes are not fed by large (kpc or larger) discs but rather by flows with a small specific angular momentum.
- We also noted that SMBH outflows in a realistic, i.e., aspherical, situation may pump turbulence (differential motions) in the bulge. Turbulence is known to hinder star formation. Therefore we believe that AGN feedback not only expels the gas from the galaxy but it may also reduce the amount of mass turned into stars during bulge formation.

9 ACKNOWLEDGMENTS

The authors thank Andrew King for illuminating discussions and comments on the draft of the paper. Volker Springel is thanked for help with Gadget and comments on an early draft of the paper. Theoretical Astrophysics research at the University of Leicester is supported by a STFC Rolling grant.

REFERENCES

Bondi H., 1952, MNRAS, 112, 195

- Bondi H., Hoyle F., 1944, MNRAS, 104, 273
- Churazov E., Sunyaev R., Forman W., Böhringer H., 2002, MNRAS, 332, 729
- Di Matteo T., Springel V., Hernquist L., 2005, Nature, 433, 604
- Dobbs C. L., Bonnell I. A., Clark P. C., 2005, MNRAS, 360, 2
- Fabian A. C., 1999, MNRAS, 308, L39
- Ferrarese L., Côté P., Dalla Bontà E., et al., 2006, ApJL, 644, L21
- Ferrarese L., Merritt D., 2000, ApJL, 539, L9
- Gebhardt K., Bender R., Bower G., et al., 2000, ApJL, 539, L13
- Goodman J., 2003, MNRAS, 339, 937
- Gültekin K., Richstone D. O., Gebhardt K., et al., 2009, ApJ, 698, 198
- Häring N., Rix H.-W., 2004, ApJL, 604, L89
- Hu J., 2009, ArXiv e-prints
- Kereš D., Katz N., Weinberg D. H., Davé R., 2005, MNRAS, 363, 2
- King A., 2003, ApJL, 596, L27
- King A., 2005, ApJL, 635, L121
- King A. R., Lubow S. H., Ogilvie G. I., Pringle J. E., 2005, MNRAS, 363, 49
- King A. R., Pounds K. A., 2003, MNRAS, 345, 657
- King A. R., Pringle J. E., 2006, MNRAS, 373, L90
- Krolik J. H., Begelman M. C., 1988, ApJ, 329, 702
- Mac Low M.-M., Klessen R. S., 2004, Reviews of Modern Physics, 76, 125
- Magorrian J., Tremaine S., Richstone D., et al., 1998, AJ, 115, 2285
- McKee C. F., Ostriker E. C., 2007, ARA&A, 45, 565
- Nayakshin S., Cha S.-H., Hobbs A., 2009a, MNRAS, 397, 1314
- Nayakshin S., Cuadra J., Springel V., 2007, MNRAS, 379, 21
- Nayakshin S., Wilkinson M. I., King A., 2009b, MNRAS, 398, L54
- Sazonov S. Y., Ostriker J. P., Ciotti L., Sunyaev R. A., 2005, MNRAS, 358, 168
- Shakura N. I., Sunyaev R. A., 1973, A&A, 24, 337
- Sijacki D., Springel V., di Matteo T., Hernquist L., 2007, MNRAS, 380, 877
- Silk J., Rees M. J., 1998, A&A, 331, L1
- Springel V., Di Matteo T., Hernquist L., 2005, MNRAS, 361, 776
- Tremaine S., Gebhardt K., Bender R., et al., 2002, ApJ, 574, 740
- Wehner E. H., Harris W. E., 2006, ApJL, 644, L17